Energy materials

High-purity LiFePO$_4$ prepared by a rapid one-step microwave-assisted hydrothermal synthesis

Carlos A. G. Bezerra[1], Rogério A. Davoglio[1], Sonia R. Biaggio[1], Nerilso Bocchi[1,*] (iD), and Romeu C. Rocha-Filho[1]

[1] *Departamento de Química, Universidade Federal de São Carlos, Caixa Postal 676, São Carlos, SP 13560-970, Brazil*

ABSTRACT

A microwave-assisted hydrothermal synthesis route to prepare LiFePO$_4$ (LFP) in a very short time and under a low temperature is proposed. Only 10 min at 200 °C was sufficient to produce a high-purity, single-phase LFP, with no need to perform a thermal treatment as a second step that is usual to enhance the structural properties of the material. The obtained LFP was structurally characterized by XRD, HR-TEM and FTIR spectroscopy and morphologically analyzed by SEM. Electrochemical impedance spectroscopy data allowed the estimation of the diffusion coefficient for the lithium ions ($D_{Li}^+ = 2.0 \times 10^{-14}$ cm^2 s^{-1}) in the LFP structure during the redox reactions related to the charge and discharge processes that occur in a Li-ion battery. Preliminary galvanostatic charge and discharge tests of the prepared LFP as a cathode in a Li-ion cell were carried out in a 1.0 mol L^{-1} LiPF$_6$ EC/DMC 1:1 (*V/V*) electrolyte solution, allowing the estimation of the initial specific capacity (126 mA h g^{-1} at 0.1 C) and coulombic efficiency (94–99%). Hence, the here-reported rapid, clean and facile one-step synthesis of LFP allows the production of a material that has excellent structural properties and a promising electrochemical response, with significant savings in time and energy.

Introduction

The decrease of oil reserves worldwide, allied with climate changes due to global warming, has motivated the search for new, renewable and clean sources of energy [1]. This search for alternative energy sources has been driven mainly by the automotive sector, which is continuously expanding and has been one of the main drivers for environmental pollution [2]. Hence, electric vehicles, whose energy source for their engines is typically a lithium-ion battery bank [1–4], have been produced more and more to replace the traditional automobiles powered by internal combustion engines.

Handling Editor: Christopher Blanford.

Address correspondence to E-mail: bocchi@ufscar.br

Among the lithium-ion battery components, the cathode material is known to be a key item that determines the performance and cost of the device [4–6]. A broad variety of materials has been proposed by many research groups for cathodes in Li-ion batteries. Among these materials, lithiated iron phosphate ($LiFePO_4$), first investigated by Padhi et al. [7], has presented promising results [4, 8]. $LiFePO_4$ is considered a good electrode material because of its high values of theoretical and experimental specific capacities [9, 10], low toxicity and high electrochemical stability [11], besides being benign and produced from low-cost precursors. However, $LiFePO_4$ presents low ionic and electronic conductivities (which lead to a decrease in the experimental specific capacity) as well as coulombic efficiency losses during long-term charge–discharge cycling [12, 13].

New synthesis methodologies have been proposed to enhance the conductivity of $LiFePO_4$, focusing on the decrease in particle size, the production of a carbonaceous coating and the obtention of crystalline and high-purity materials [14–24]. Traditionally $LiFePO_4$ is produced by means of solid-state synthesis, when the solid precursor materials are mixed and submitted to different heating steps at temperatures varying in the range of 350–800 °C, in procedures that may last up to 24 h [25, 26]. Although solid-state synthesis may lead to products that present good structural and electrochemical properties, the associated high temperatures and long heating periods make it energetically expensive. In this context, significant energy savings can be attained by the use of hydrothermal synthesis [27–30] since the precursors (dissolved and mixed in aqueous solutions) are submitted to lower temperatures (around 200 °C) during 5–18 h [31, 32]. The hydrothermal methodology allows the production of nanostructured and high-purity $LiFePO_4$ that leads to a cathode material with high electrochemical performance [33]. Although the latter presents lower energy consumption compared to solid-state synthesis, both methods involve long heating periods due to the inefficient heat exchange (by heat conduction, irradiation and convection) between the heat source and the reaction system. Therefore, the coupling of the hydrothermal methodology with microwave heating improves the heat-transfer efficiency mainly due to the fact that the heat exchange occurs at the molecular level, as a consequence of the direct interaction between microwave radiation and reactants, leading to a

significant reduction of the synthesis time [34–38]. For example, Niu et al. [39] produced high-purity $LiFePO_4$ in a two-step procedure, *i.e.*, microwave-assisted hydrothermal synthesis at 180 °C for 1 h, followed by a thermal treatment (TT) at 700 °C for 2 h in a reducing atmosphere. Gao et al. [40] also used a two-step procedure to produce $LiFePO_4$, but the microwave-assisted hydrothermal synthesis was carried out at 160 °C for 20 min (with addition of ascorbic acid to the precursors as reducing agent) and the obtained product was submitted to TT at 700 °C under a nitrogen atmosphere for 3 h.

On top of the lower energy consumption and diminutive synthesis time, most works involving microwave-assisted hydrothermal synthesis have been focusing on enhancing the electrochemical performance of $LiFePO_4$ as cathode material for lithium-ion batteries by covering its particles with a thin conducting layer of carbon. Commonly, this carbonaceous layer is obtained by adding organics to the reaction medium and submitting them to TT in a controlled reducing atmosphere; this leads to a final material with an increased conductivity and thus enhanced electrochemical properties. Despite the excellent results attained with such materials, the second step in their synthesis (TT) causes an increase in the energy consumption and reaction time, which weigh negatively when large large-scale applications are considered. Besides, during TT some undesirable compounds and agglomerates of $LiFePO_4$ particles might be formed, which limit the diffusion of Li ions in the olivine structure, leading to a decreased electrochemical performance [14, 41]. In this sense, Yang et al. [42] investigated the synthesis of $LiFePO_4$ by the microwave-assisted hydrothermal method using classic inorganic precursors and without TT afterward, obtaining a material with good electrochemical performance. Nevertheless, there is not much reported on "one-step" synthesis of $LiFePO_4$, thus leaving open opportunities for investigations on the preparation of this pure material, with adequate crystalline structure and good electrochemical properties, without applying a posterior TT.

In this work, we further investigate the one-step methodology to obtain single-phase high-purity $LiFePO_4$ by a rapid microwave-assisted hydrothermal synthesis under a low temperature, with no posterior TT. The as-obtained product was characterized: structurally, by X-ray diffractometry (XRD) and FTIR spectroscopy; structurally and

morphologically, by transmission electron microscopy (TEM) and scanning electron microscopy (SEM); electrochemically, by cyclic voltammetry (CV), electrochemical impedance spectroscopy (EIS) and charge–discharge tests as a cathode in a Li-ion cell.

Materials and methods

LiFePO$_4$ synthesis

For the LiFePO$_4$ synthesis, the precursor materials were mixed in a Li:Fe:P 3:1:1 mol ratio. First of all, lithium acetate (CH$_3$CO$_2$Li.2H$_2$O 98%, Sigma-Aldrich) was dissolved in deionized water, and phosphoric acid (H$_3$PO$_4$ 85%, Synth) was added to this solution, at room temperature. A white precipitate, typical of Li$_3$PO$_4$, was formed and the mixture was stirred for 20 min with a magnetic bar and a N$_2$ flow through it. Iron sulfate (FeSO$_4$.7H$_2$O 99%, Sigma-Aldrich) was then added to the reaction mixture, which was kept under stirring and N$_2$ bubbling for additional 10 min. Then, approximately 20 mL of the resulting greenish and viscous mixture was introduced into a 30-mL borosilicate reaction vessel and heated at 200 °C for 10 min under microwave radiation, in a Monowave 400 (Anton Paar) reactor. The obtained product was washed several times with deionized water (up to neutral pH) and then dried in an oven at 60 °C for 12 h, resulting in a greenish powder as the final reaction product.

It is important to mention that this described procedure was repeated several times in order to obtain an appreciable amount of LiFePO$_4$ (few grams); FTIR spectra of LiFePO$_4$ samples synthesized in the different runs did not show significant variations.

Structural and morphological characterization

XRD spectra were obtained with a Rigaku D/MAX-2000PC diffractometer using a Cu Kα radiation source at 40 kV/150 mA. From the obtained data, acquired in the 5–80° range at a rate of 1° min^{-1}, the crystalline phase was identified by comparison with Joint Committee of Powder Diffraction Standards (JCPDS) data. FTIR spectra were acquired from 400 to 4000 cm^{-1}, using a Thermo Scientific model Nicolet 6700 spectrometer.

SEM images were obtained with a FEI Magellan 400L (2 kV) microscope; TEM and selected-area electron diffraction (SAED) images were acquired with a Supra-35 ZEISS FESEM system in a high-resolution FEI (MET-AR) Tecnai G^2 (200 kV) microscope. The SEM and TEM results were analyzed with the ImageJ software [43].

Electrochemical characterization

The working electrodes were prepared as a composite of LiFePO$_4$/carbon black/PVDF at a 70:20:10 mass ratio in cyclopentanone. The resulting composite slurry was applied on Pt and Al current collectors and then casted in a vacuum oven at 120 °C. The Pt and Al electrodes were employed, respectively, for CV and galvanostatic charge–discharge/EIS tests. Assembling of the electrochemical cells was carried out in a Labconco® model 506,000 glove box under an argon (99.999%) atmosphere. Metallic lithium was used as the counter and reference electrodes for the CV tests (0.1 mV s^{-1}) in a 1.0 mol L^{-1} LiClO$_4$ EC/DMC 1:1 (V/V) electrolyte solution in the potential range of 2.4–4.2 V versus Li/Li$^+$.

The charge–discharge tests were performed in a 1.0 mol L^{-1} LiPF$_6$ EC/DMC 1:1 (V/V) electrolyte solution using a Swagelok®-type cell at various current densities, keeping the potential window between 2.4 and 4.5 V versus Li/Li$^+$. Both CV and charge–discharge experiments were carried out using a Metrohm-Autolab PGSTAT204 interface.

The EIS measurements were carried out in a Swagelok®-type cell having as electrolyte a 1.0 mol L^{-1} LiPF$_6$ EC/DMC 1:1 (V/V) solution, using an Autolab PGSTAT20 interface. For such, a 10 mV peak-to-peak AC signal, from 10 kHz to 10 mHz, was applied at the open-circuit potential (OCP).

All electrochemical measurements were always carried out in triplicate.

Results and discussion

Structural and morphological analyses of the synthesized LiFePO$_4$

An obtained XRD spectrum, characteristic of the LFP samples, is presented in Fig. 1a. Well-defined peaks can be seen at 17.2°, 20.9°, 25.7°, 30.0°, 32.2°, 35.6° and 52.6°, which were indexed to the diffraction lines

Figure 1 a Typical X-ray diffractogram and **b** FTIR spectrum of a LiFePO$_4$ sample obtained by microwave-assisted hydrothermal synthesis at 200 °C for 10 min. The inset in **a** corresponds to the XRD spectrum of the JPCDS 40–1499 crystallographic card.
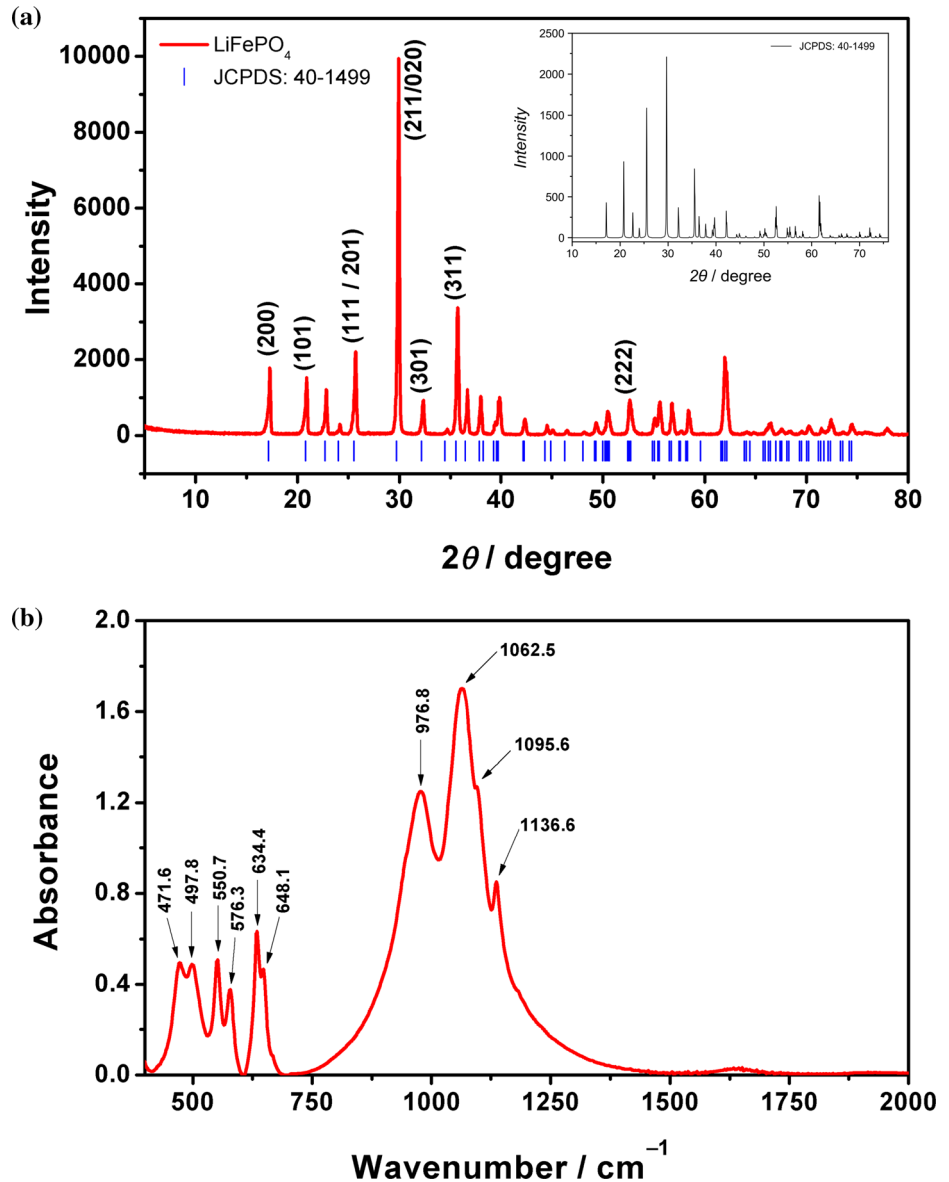
(200), (101), (111/201), (211/020), (301), (311) and (222), respectively, of the orthorhombic crystalline phase of pure LiFePO$_4$ (JPCDS 40–1499; see inset in Fig. 1a). A high degree of crystallinity for the synthesized material can be inferred from the high definition of the peaks, whereas the more intense peak at 30.0° (peak 211) is an indication of the particle preferential growth along the {001} and {100} planes, or *ac* plane in the orthorhombic LiFePO$_4$ crystal (space group Pnma), a fact that favors Li$^+$ diffusion along the shorter plane (or *b*-axis of the crystal) [44]. Based on this more intense peak, the mean size (L_m) of the LiFePO$_4$ particles was calculated using the Debye–Scherrer equation:

$$L_m = \frac{K\lambda}{\beta \cos \theta} \tag{1}$$

where K is a constant (0.94), λ the X-ray wavelength (1.5418 nm) and β the width (in radians) at the half-height of the more intense peak, whose Bragg angle is θ. The thus obtained nanometric mean size of the synthesized LiFePO$_4$ particles, 41.8 nm, represents a short diffusional path for the lithium ions in the LFP structure and might contribute positively for its electrochemical performance when tested as a cathode material in Li-ion batteries.

Figure 1b shows a typical FTIR spectrum for the as-synthesized LiFePO$_4$. The predominance of the internal vibrational modes of the phosphate group

can be seen in the 400–2000 cm^{-1} region of the spectrum [45]. According to the interactions of the atoms in PO_4^{3-} with the lithium and iron ions in the crystal, the position and intensity of the FTIR bands may change significantly and lead to information on the crystallinity, purity and composition of the obtained material [45–49].

Thus, the well-defined bands in the region of 400–690 cm^{-1} are signatures of the vibrational modes v_2 and v_4 of the phosphate group, whereas the bands in the region of 700–1139 cm^{-1} refer to the internal vibrational modes v_1 and v_3 of the phosphate group in the LiFePO$_4$ structure [45]. The lack of bands in the region of 700–900 cm^{-1} is a strong indication of the high purity of the obtained material, since bands in this region of the spectrum are characteristic of other phosphate complexes such as $P_2O_7^{4-}$, $P_3O_{10}^{5-}$ and FePO$_4$, which could be formed as byproducts during the synthesis [47, 48].

The morphology and mean size distribution of the LFP particles are presented in Fig. 2a and b, respectively. The morphology observed for this material is basically globular; its mean particle size

(57.4 ± 1.8 nm) was calculated based on the lognormal distribution presented in Fig. 2b. Although this value is higher than the one obtained using the Debye–Scherrer Eq. (41.8 nm), the results indicate a good agreement between the methods. Additionally, as can be inferred from Fig. 2b, the majority of the LFP particles present sizes close to the mean value; this narrow distribution of particle size attained by the herein-proposed synthesis may represent an advantage in comparison with other methods, since no further processes are needed to attain such particle size homogeneity [28]. On the other hand, it is clear from the TEM image (Fig. 2c) that the LFP sample is highly crystalline, with a tendency of crystal growth along one preferential plane. Furthermore, the dotted pattern of the SAED image in Fig. 2d is another evidence for the monocrystalline domain of the synthesized LFP sample, with two main diffraction lines: 211 and 311. In summary, both the TEM and SAED results corroborate the XRD findings presented in Fig. 1a.
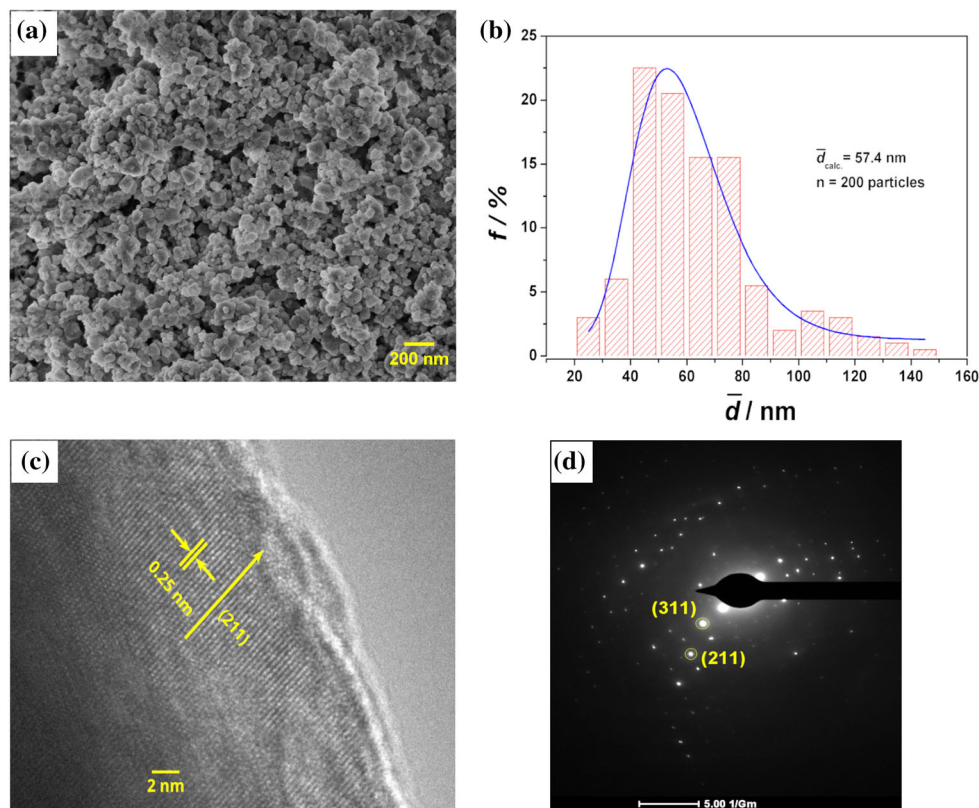

Figure 2 **a** SEM micrograph and related **b** particle size distribution (for 200 particles), **c** TEM image and **d** SAED image for the LiFePO$_4$ sample obtained by microwave-assisted hydrothermal synthesis at 200 °C for 10 min.
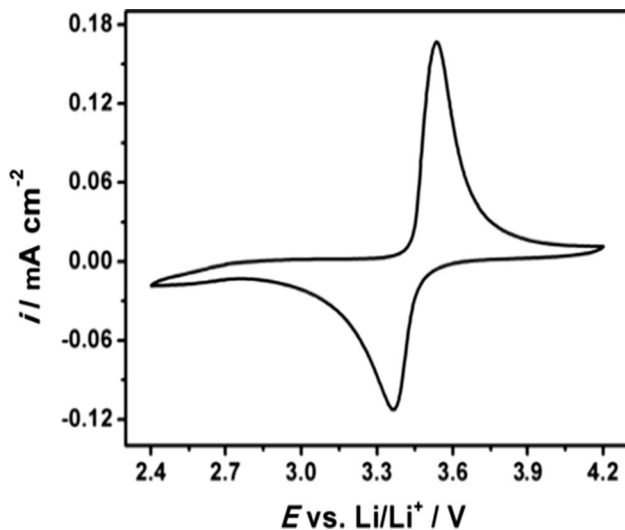
Electrochemical characterization

The electrochemical activity of the obtained LFP was initially evaluated by CV at a slow sweep rate (0.1 mV s^{-1}) in the potential range of 2.4–4.2 V versus Li/Li$^+$ in a 1.0 mol L^{-1} LiClO$_4$ EC/DMC 1:1 (V/V) electrolyte solution. As illustrated in Fig. 3, the typical obtained voltammogram presents well-defined oxidation and reduction peaks at 3.5 and 3.4 V, respectively, corresponding to the Fe^{3+}/Fe^{2+} redox reactions of a LiFePO$_4$ cathode that occur during the charging and discharging processes in a lithium-ion cell.

The charging process occurs simultaneously with the oxidation of Fe^{2+} and extraction of Li$^+$ from the olivine structure (Eq. 2), while Fe^{3+} is reduced and Li$^+$ inserted in the material structure during the discharging process (Eq. 3).

$$Li_xFePO_4 \rightarrow FePO_4 + xLi^+ + xe^- \quad (2)$$

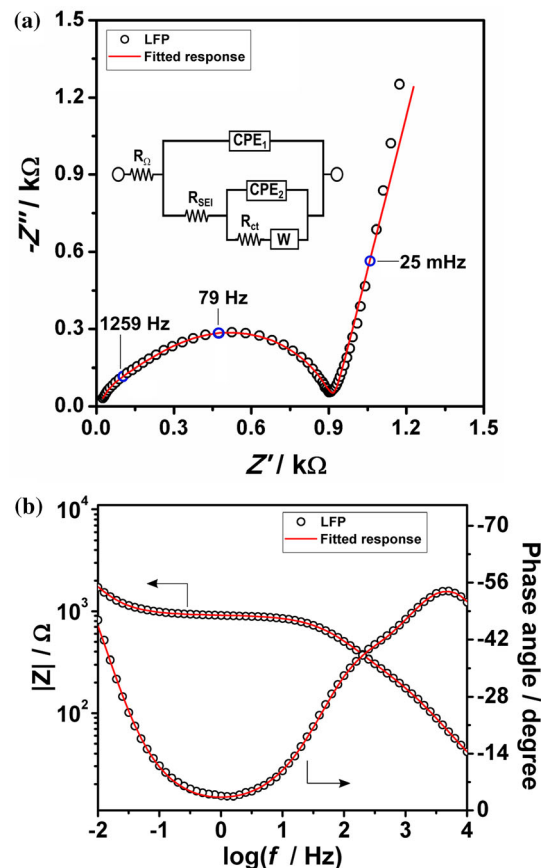$$FePO_4 + xLi^+ + xe^- \rightarrow Li_xFePO_4. \quad (3)$$
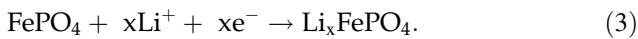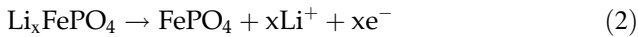
The potential value between the oxidation and reduction peaks is 3.45 V versus Li/Li$^+$, which approximately corresponds to the OCP of the working electrode; the two phases LiFePO$_4$ and FePO$_4$, characteristic of the charging and discharging processes, coexist around this value of the electrode potential [50, 51]. The peak-potential separation for the redox process is about 100 mV, indicating that the

prepared electrode presents good reversibility. Besides that, the absence of additional voltammetric peaks in Fig. 3 is another evidence that other Fe compounds (byproducts or impurities) were not formed during the LFP synthesis and that the electrolyte is electrochemically stable in the considered potential range.

The obtained EIS data were analyzed to access information on processes that occur in the phases and at the LiFePO$_4$/electrolyte interface. Typical EIS data obtained for the here-synthesized LiFePO$_4$ are presented as complex plane (or Nyquist) and Bode plots in Fig. 4a and 4b, respectively. The semicircle in the Nyquist plot can be attributed to a parallel RC circuit relaxing at the highest frequencies in the analyzed system. The linear region at lower frequencies can be attributed to diffusional or capacitive processes

Figure 3 Typical cyclic voltammetric profile at 0.1 mV s^{-1} for the LiFePO$_4$ sample obtained by microwave-assisted hydrothermal synthesis at 200 °C for 10 min. Electrolyte solution: 1.0 mol L^{-1} LiClO$_4$ in EC/DMC 1:1 (V/V).

Figure 4 a Typical complex plane and b Bode plots for the LiFePO$_4$ (LFP) sample obtained by microwave-assisted hydrothermal synthesis at 200 °C for 10 min. The equivalent circuit whose response (red lines) fitted the experimental EIS data is shown as an inset in a. Electrolyte solution: 1.0 mol L^{-1} LiPF$_6$ in EC/DMC 1:1 (V/V).

occurring in the phases or at the interfaces. Therefore, an equivalent electric circuit (EEC) model (see inset in Fig. 4a) was proposed to simulate and interpret the obtained impedance data, with the following elements: the ohmic resistance (R_Ω) related to the ionic resistance of the electrolyte; the charge-transfer resistance (R_{ct}) at the LFP/electrolyte interface; the resistance associated with a solid electrolyte interface (R_{SEI}) formed on the electrode [52]; non-ideal capacitive processes (CPE_1 and CPE_2) related to changes in the thickness, roughness and porosity of the electrode material [53]—CPE_1 was attributed to the double-layer charge at the $LiFePO_4$/electrolyte interface and CPE_2 to the spatial capacitance defined by the LFP layer; the Warburg impedance (W) related to Li-ion diffusion in the electroactive-material channels.

The good fitting of the continuous lines in Fig. 4a and b to the EIS data indicates a good agreement between the response of the proposed EEC and the experimental data; this is confirmed by the low Chi-square value of 3.7×10^{-5} for this fitting. The fitted values for the different EEC elements are listed in Table 1.

The analysis of the impedance data in the low-frequency region allowed estimating the diffusion coefficient of Li ions in the LFP structure. Indeed, a linear relationship between the real impedance values and those of the inverse of the square root of the angular frequency was obtained (Fig. 5); the Li-ion diffusion coefficient was calculated from the slope (σ_w) of this line, using the following equation [54, 55]:

$$D_{Li}^+ = \frac{R^2 T^2}{2 A^2 n^4 F^4 C^2} \sigma_W^2 \qquad (4)$$

where D_{Li^+} is the Li-ion diffusion coefficient ($cm^2\ s^{-1}$), R the universal gas constant (8.314 J K^{-1} mol^{-1}), T the thermodynamic temperature (298 K), A the electrode geometric area (0.785 cm^2), F the Faraday constant (96,485 C mol^{-1}), C the concentration of Li^+ (0.0228 mol cm^{-3}, assuming a mass density of 3.6 g cm^{-3} and a molar mass of 157.78 g mol^{-1} for $LiFePO_4$) and n the number of electrons
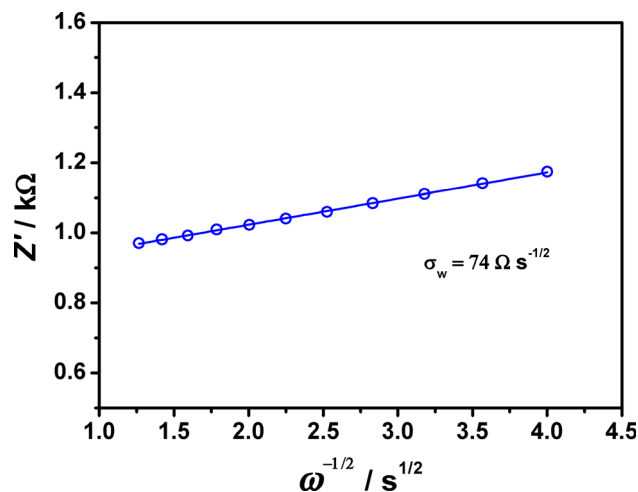
Figure 5 Linear relationship between Z' and $\omega^{-1/2}$ in the low-frequency region (0.1–0.01 Hz) for the $LiFePO_4$ sample obtained by microwave-assisted hydrothermal synthesis at 200 °C for 10 min.

transferred in the redox reaction of the Fe^{3+}/Fe^{2+} redox couple.

A D_{Li+} value of 2.0×10^{-14} $cm^2\ s^{-1}$ was obtained for the here-synthesized LFP sample, in agreement with other values reported for high-performance $LiFePO_4$ electrodes [12, 44, 56, 57]. This result may be related to the particle preferential growth along the {001} and {100} planes, which favors Li^+ diffusion along the shorter {010} plane. Li-ion diffusion takes place only along the b-axis during charge and discharge, and the charge transfer takes place mainly on the ac plane. A decrease in the diffusion length along the {010} plane makes the insertion/extraction process faster and, consequently, improves the electrochemical performance of the electrode [58, 59]. The proportion between the {001} and {100} planes can be estimated from the peak intensity ratio I(020)/I(200) in the X-ray diffractograms of $LiFePO_4$ [60] and was proposed to give an idea about the preferential direction of the particle growth. In the present work, the ratio I(020)/I(200) that is shown in Fig. 1 points toward the preferential growth along the ac plane.

Table 1 Values associated with the different elements of the equivalent electric circuit (see inset in Fig. 4a) whose response was fitted to the EIS data for the $LiFePO_4$ sample obtained by microwave-assisted hydrothermal synthesis at 200 °C for 10 min (Fig. 4)

| R_Ω/Ω	CPE_1/mF s^{n-1}	n	R_{ct}/Ω	CPE_2/mF s^{n-1}	n	R_{SEI}/Ω
11.8	4.18×10^{-6}	0.79	356	9.03×10^{-6}	0.83	516

Chi-square: 3.7×10^{-5}

Galvanostatic charge and discharge tests

Preliminary charge and discharge tests were carried out to assess the performance of the here-synthesized LiFePO₄. Figure 6a shows typical charge and discharge profiles obtained at the 0.1 C rate in the potential range of 2.4–4.5 V versus Li/Li⁺ for the cell:

$$Li \,|\, 1.0\,mol\,L^{-1}\,LiPF_6,\,EC-DMC\,|\,LiFePO_4\,|\,Al.$$

The chronopotentiometric profiles obtained for the LFP electrode present a neat plateau around 3.45 V, related to the redox processes represented by Eqs. 2 and 3; its initial specific capacity was calculated as 126 mA h g⁻¹ at a discharge rate of 0.1 C. Besides, from the potential gap values between the charge and
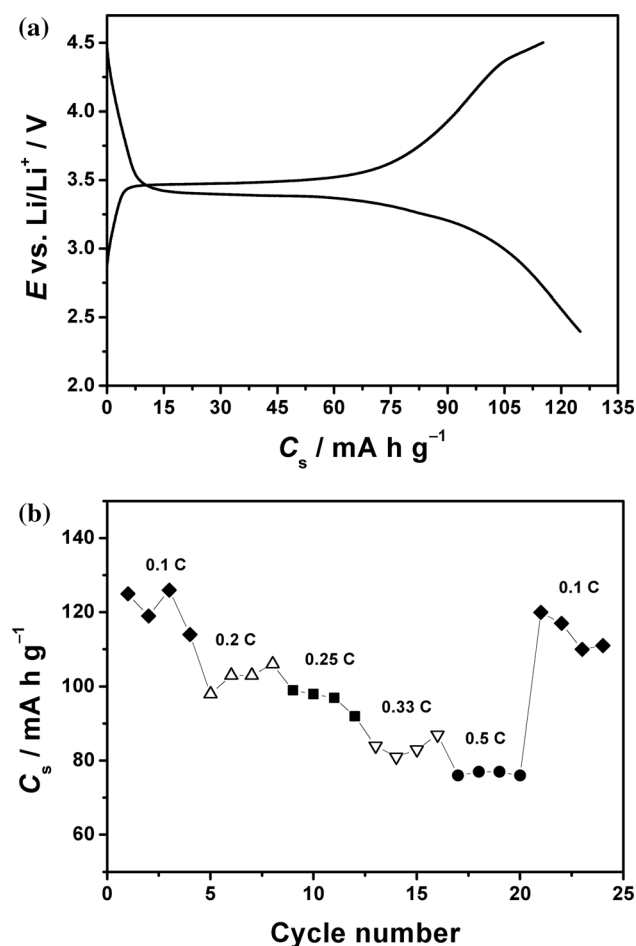
discharge plateaus (70 mV), one can infer a high reversibility for this electrode prepared by the microwave-assisted hydrothermal method.

The LFP electrode was submitted to several charge–discharge rates (0.1, 0.2, 0.25, 0.33 and 0.5 C) to assess its rate capability in comparison with the 0.1 C rate. The respective results are presented in Fig. 6b. When the charge–discharge rate was doubled to 0.2 C, the charge retention from the initial value (126 mA h g⁻¹) was of 86%, while it decreased to 62% when the charge–discharge rate was increased fivefold (to 0.5 C). After these successive charge–discharge cycles, the electrode was submitted again to the lowest charge–discharge rate (0.1 C), when 95% of its initial charge was recovered, attesting once again the excellent properties of the here-prepared material.

Finally, it is noteworthy that the electrochemical performance of the obtained LFP electrode is comparable to that of others whose LFP was similarly synthesized (MWH methodology) and then submitted (two-step process) [39, 40, 61–63] or not (one-step process) [42] to a TT to obtain better structural properties or to increase its conductivity by generating a carbon coating on its particles (Table 2). Analyzing this table, it is clear that the rapid, clean and facile one-step synthesis here reported leads to the production of a competitive LFP with excellent structural characteristics and good electrochemical properties at shorter times and under a lower temperature. These results may open the possibility of applying the thus obtained LFP as a cathode material of lithium-ion batteries without the addition of a carbonaceous material and the further heat treatment that increases the synthesis time and final cost of the material, despite the eventual increase in the values of specific capacity after this two-step process [40, 61–63].

Conclusions

A rapid one-step procedure based on a microwave-assisted hydrothermal reaction was successfully employed to prepare LiFePO₄ (LFP) under a low temperature (10 min at 200 ℃). High-purity and single-phase LFP with good electrochemical properties was obtained, without submitting it to a posterior thermal treatment as is usual in other hydrothermal synthesis routes to enhance the properties of the

Figure 6 a Typical charge and discharge profiles at the 0.1 C rate and **b** specific capacity (C_s) as a function of different charge–discharge rates (indicated in the figure) for the LiFePO₄ sample obtained by microwave-assisted hydrothermal synthesis at 200 ℃ for 10 min. Electrolyte solution: 1.0 mol L⁻¹ LiPF₆ in EC/DMC 1:1 (*V/V*).

Table 2 Comparison of the values of specific capacity obtained at 0.1 C for the synthesized LFP with those reported for other similarly synthesized LFPs

Authors	Precursors used	Synthesis time/min	Synthesis temperature/°C	Thermal treatment	Initial specific capacity/ (mA h g^{-1})
Niu et al. [39]	$NH_4H_2PO_3$, $FeSO_4.7H_2O$, Li_2CO_3 and polyethylene glycol	60	180	700 °C for 2 h in H_2/Ar atmosphere after addition of glucose	99.6
Gao et al. [40]	$FeSO_4$, LiOH, H_3PO_4 and ascorbic acid	20	160	700 °C for 3 h in N_2 atmosphere after addition of glucose	165
Yang et al. [42]	$LiOH.H_2O$, $FeSO_4.7H_2O$ and H_3PO_4	5	200	None	136
Murugan et al. [61]	$FeSO_4$, LiOH, H_3PO_4 and glucose	15	235	700 °C for 1 h in H_2/Ar atmosphere	146
Chen et al. [62]	LiH_2PO_4 and $C_6H_5FeO_7$	20	200	700 °C for 1 h in H_2/Ar atmosphere after addition of saccharose	148
Zhang & Liang [63]	$FeSO_4$, LiOH, H_3PO_4 and ascorbic acid	4	220	700 °C for l h in H_2/Ar atmosphere	152
This work	$FeSO_4$, CH_3CO_2Li and H_3PO_4	10	200	None	126

material. The diffusion coefficient of lithium ions in the LFP structure during the charge and discharge processes was estimated as 2.0×10^{-14} cm^2 s^{-1}. Preliminary charge and discharge tests of the here-prepared LiFePO$_4$ as a cathode in a Li-ion cell allowed the estimation of its initial specific capacity as 126 mA h g^{-1} at the 0.1 C rate. Thus, the rapid, clean and facile one-step synthesis of LFP here reported allows the production of a material that has excellent structural and promising electrochemical properties, with significant savings in time and energy.

Acknowledgements

Compliance with ethical standards

Conflict of interest The authors declare that they have no known competing financial interests or personal relationships that could have appeared to influence the work reported in this paper.

References

[1] Larcher D, Tarascon JM (2015) Towards greener and more sustainable batteries for electrical energy storage. Nat Chem 7:19–29

[2] Tie SF, Tan CW (2013) A review of energy sources and energy management system in electric vehicles. Renew Sust Energ Rev 20:82–102

[3] Weiss M, Patel MK, Junginger M, Perujo A, Bonnel P, Grootveld G (2012) On the electrification of road transport: learning rates and price forecasts for hybrid-electric and battery-electric vehicles. Energ Policy 48:374–393

[4] Nitta N, Wu F, Lee JT, Yushin G (2015) Li-ion battery materials: present and future. Mater Today 18:252–264

[5] Goodenough JB, Kim Y (2010) Challenges for rechargeable li batteries. Chem Mater 22:587–603

[6] Manthiram A (2011) Materials challenges and opportunities of lithium ion batteries. J Phys Chem Lett 2:176–184

[7] Padhi AK, Nanjundaswamy KS, Goodenough JB (1997) Phospho-olivines as positive-electrode materials for rechargeable lithium batteries. J Electrochem Soc 144:1188–1194

[8] Kurzweil P (2015) Lithium battery energy storage: state of the art including lithium-air and lithium-sulfur systems. In: Moseley PT, Garche J (eds) Electrochemical Energy Storage for Renewable Sources and Grid Balancing. Elsevier, Amsterdam, pp 269–307

[9] Chen J, Vacchio MJ, Wang S, Chernova N, Zavalij PY, Whittingham MS (2008) The hydrothermal synthesis and characterization of olivines and related compounds for electrochemical applications. Solid State Ionics 178:1676–1693

[10] Huang Z, Luo P, Wang D (2017) Preparation and characterization of core-shell structured LiFePO4/C composite using a novel carbon source for lithium-ion battery cathode. J Phys Chem Solids 102:115–120

[11] Qiao YQ, Feng WL, Li J, Shen TD (2017) Ultralong cycling stability of carbon-nanotube/LiFePO$_4$ nanocomposites as electrode materials for lithium-ion batteries. Electrochim Acta 232:323–331

[12] Prosini PP, Lisi M, Zane D, Pasquali M (2002) Determination of the chemical diffusion coefficient of lithium in LiFePO$_4$. Solid State Ionics 148:45–51

[13] Zaghib K, Guerfi A, Hovington P, Vijh A, Trudeau M, Mauger A, Goodenough JB, Julien CM (2013) Review and analysis of nanostructured olivine-based lithium rechargeable batteries: status and trends. J Power Sources 232:357–369

[14] Zhang L, Xiang H, Zhu X, Yang W, Wang H (2012) Synthesis of LiFePO4/C composite as a cathode material for lithium-ion battery by a novel two-step method. J Mater Sci 47:3076–3081. https://doi.org/10.1007/s10853-011-6139-7

[15] Qiu Y, Geng Y, Yu J, Zuo X (2014) High-capacity cathode for lithium-ion battery from LiFePO$_4$/(C + Fe$_2$P) composite nanofibers by electrospinning. J Mater Sci 49:504–509. https://doi.org/10.1007/s10853-013-7727-5

[16] Yang Z, Dai Y, Wang S, Yu J (2016) How to make lithium iron phosphate better: a review exploring classical modification approaches in-depth and proposing future optimization methods. J Mater Chem A 4:18210–18222

[17] Smecellato PC, Davoglio RA, Biaggio SR, Bocchi N, Rocha-Filho RC (2017) Alternative route for LiFePO4 synthesis: Carbothermal reduction combined with microwave-assisted solid-state reaction. Mater Res Bull 86:209–214

[18] Zhao C, Wang L, Wu H, Chen J, Gao M (2018) Ultrafast fabrication of LiFePO4 with high capacity and superior rate cycling performance for lithium ion batteries. Mater Res Bul 97:195–200

[19] Hu G, Xie X, Cao Y, Xu L, Du K, Wang W, Peng Z (2019) Ultrasonic-assisted synthesis of LiFePO4/C composite for lithium-ion batteries using iron powder as the reactant. J Alloy Compd 773:1165–1171

[20] Xie X, Hu G, Cao Y, Du K, Gan Z, Xu L, Wang Y, Peng Z (2019) Rheological phase synthesis of Fe$_2$P$_2$O$_7$/C composites as the precursor to fabricate high performance LiFePO4/C composites for lithium-ion batteries. Ceram Inter 45:12331–12336

[21] Rajoba SJ, Jadhav LD, Kalubarme RS, Yadav SN (2019) Influence of synthesis parameters on the physicochemical and electrochemical properties of LiFePO4 for Li-ion battery. J Alloy Compd 774:841–847

[22] Zhou W, Liu C, Wen Z, Xu J, Han T, Li G, Huang D, Liang X, Lan Z, Ning H, Huang H, Guo J (2019) Effects of defect chemistry and kinetic behavior on electrochemical properties for hydrothermal synthesis of LiFePO4/C cathode materials. Mater Chem Phys 227:56–63

[23] Sun J, Li Z, Ren X, Wang L, Liang G (2019) High volumetric energy density of LiFePO4/C microspheres based on xylitol-polyvinyl alcohol complex carbon sources. J Alloy Compd 773:788–795

[24] Omidi AH, Babaei A, Ataie A (2020) Low temperature synthesis of nanostructured LiFePO4/C cathode material for lithium ion batteries. Mater Res Bull 125:110807

[25] Jugović D, Uskoković D (2009) A review of recent developments in the synthesis procedures of lithium iron phosphate powders. J Power Sources 190:538–544

[26] Calderón CA, Thomas JE, Lener G, Barraco DE, Visintin A (2017) Electrochemical comparison of LiFePO4 synthesized by a solid-state method using either microwave heating or a tube furnace. J Appl Electrochem 47:1179–1188

[27] Bao L, Xu G, Sun X, Zeng H, Zhao R, Yang X, Shen G, Han G, Zhou S (2017) Mono-dispersed LiFePO4@C core-shell [001] nanorods for a high power Li-ion battery cathode. J Alloy Compd 708:685–693

[28] Milev A, George L, Khan S, Selvam P, Kamali Kannangara GS (2016) Li-ion kinetics in LiFePO4/carbon nanocomposite prepared by a two-step process: the role of phase composition. Electrochim Acta 209:565–573

[29] Bolloju S, Rohan R, Wu S-T, Yen H-X, Dwivedi GD, Lin YA, Lee JT (2016) A green and facile approach for hydrothermal synthesis of LiFePO4 using iron metal directly. Electrochim Acta 220:164–168

[30] Kumar S, Chand P, Joshi A, Singh V (2020) Modeling of electrical behavior of LiFePO4 cathode materials for lithium ion batteries. Mater Today-Proc 28:337–341

[31] Wang Y, Zhang D, Chang C, Deng L, Huang K (2014) Controllable growth of LiFePO4 microplates of (010) and (001) lattice planes for Li ion batteries: a case of the growth

manner on the Li ion diffusion coefficient and electrochemical performance. Mater Chem Phys 148:933–939

[32] Julien CM, Mauger A, Zaghib K (2011) Surface effects on electrochemical properties of nano-sized $LiFePO_4$. J Mater Chem 21:9955–9968

[33] Satyavani TVSL, Srinivas Kumar A, Subba Rao PSV (2016) Methods of synthesis and performance improvement of lithium iron phosphate for high rate Li-ion batteries: a review. Eng Sci Technol Inter J 19:178–188

[34] Tompsett Geoffrey A, Conner William C, Yngvesson KS (2006) Microwave synthesis of nanoporous materials. Chem Phys Chem 7(2):296–319

[35] Meng L-Y, Wang B, Ma M-G, Lin K-L (2016) The progress of microwave-assisted hydrothermal method in the synthesis of functional nanomaterials. Mater Today Chem 1–2:63–83

[36] Liu S, Yan P, Li H, Zhang X, Sun W (2020) One-step microwave synthesis of micro/nanoscale $LiFePO_4$/graphene cathode with high performance for lithium-ion batteries. Front Chem 8:104. https://doi.org/10.3389/fchem.2020.00104

[37] Ruiz-Jorge F, Benítez A, Fernández-García S, Sánchez-Oneto J, Portela JR (2020) Effect of fast heating and cooling in the hydrothermal synthesis on $LiFePO_4$ microparticles. Ind Eng Chem Res 59:9318–9327

[38] Su L, Jha SK, Phuah XL, Xu J, Nakamura N, Wang H, Okasinski JS, Reeja-Jayan B (2020) Engineering lithium-ion battery cathodes for high-voltage applications using electromagnetic excitation. J Mater Sci 55:12177–12190. https://doi.org/10.1007/s10853-020-04871-5

[39] Niu B, Qi E-l, Wang J-Q (2011) A simple and facile preparation of $LiFePO_4$ by a one-step microwave hydrothermal method. J Inorg Organomet P 21:906–912

[40] Gao C, Zhou J, Liu G, Wang L (2017) Microwave-assisted synthesis and surface decoration of $LiFePO_4$ hexagonal nanoplates for lithium-ion batteries with excellent electrochemical performance. J Mater Sci 52:1590–1602. https://doi.org/10.1007/s10853-016-0453-z

[41] Yuan L-X, Wang Z-H, Zhang W-X, Hu X-L, Chen J-T, Huang Y-H, Goodenough JB (2011) Development and challenges of $LiFePO_4$ cathode material for lithium-ion batteries. Energ Environ Sci 4:269–284

[42] Yang G, Ji H, Miao X, Hong A, Yan Y (2011) Crystal growth behavior of $LiFePO_4$ in microwave-assisted hydrothermal condition: from nanoparticle to nanosheet. J Nanosci Nanotechno 11(6):4781–4792

[43] Schneider CA, Rasband WS, Eliceiri KW (2012) NIH Image to ImageJ: 25 years of image analysis. Nat Methods 9:671–675

[44] Churikov A, Ivanishchev A, Ivanishcheva I, Sycheva V, Khasanova N, Antipov E (2010) Determination of lithium diffusion coefficient in $LiFePO_4$ electrode by galvanostatic and potentiostatic intermittent titration techniques. Electrochim Acta 55:2939–2950

[45] Burba CM, Frech R (2004) Raman and FTIR Spectroscopic Study of Li_xFePO_4 ($0 \le x \le 1$). J Electrochem Soc 151:A1032–A1038

[46] Ravet N, Gauthier M, Zaghib K, Goodenough J, Mauger A, Gendron F, Julien CM (2007) Mechanism of the Fe3+ reduction at low temperature for $LiFePO_4$ synthesis from a polymeric additive. Chem Mater 19:2595–2602

[47] Salah AA, Jozwiak P, Zaghib K, Garbarczyk J, Gendron F, Mauger A, Julien CM (2006) FTIR features of lithium-iron phosphates as electrode materials for rechargeable lithium batteries. Spectrochim Acta A Mol Biomol Spectrosc 65:1007–1013

[48] Zaghib K, Julien C (2005) Structure and electrochemistry of $FePO_4.2H_2O$ hydrate. J Power Sources 142:279–284

[49] Paques-Ledent MT, Tarte P (1974) Vibrational studies of olivine-type compounds—II Orthophosphates,-arsenates and-vanadates AIBIIXVO4. Spectrochim Acta A Mol Spectrosc 30:673–689

[50] Mei R, Song X, Yang Y, An Z, Zhang J (2014) Plate-like LiFePO 4 crystallite with preferential growth of (010) lattice plane for high performance Li-ion batteries. RSC Adv 4:5746–5752

[51] Lin J-H, Chen J-S (2012) Synthesis and electrochemical characterization of $LiFePO_4$/C composites prepared by the microemulsion method. Electrochim Acta 62:461–467

[52] Xi Y, Liu Y, Qin Z, Jin S, Zhang D, Zhang R, Jin M (2018) Ultralong cycling stability of cotton fabric/$LiFePO_4$ composites as electrode materials for lithium-ion batteries. J Alloy Compd 737:693–698

[53] Davoglio RA, Cabello G, Marco JF, Biaggio SR (2018) Synthesis and characterization of α-MnO_2 nanoneedles for electrochemical supercapacitors. Electrochim Acta 261:428–435

[54] Taylor S, Gileadi E (1995) Physical interpretation of the Warburg impedance. Corrosion 51:664–671

[55] Shi M, Chen Z, Sun J (1999) Determination of chloride diffusivity in concrete by AC impedance spectroscopy. Cem Concr Res 29:1111–1115

[56] Li L, Tang X, Liu H, Qu Y, Lu Z (2010) Morphological solution for enhancement of electrochemical kinetic performance of $LiFePO_4$. Electrochim Acta 56:995–999

[57] Zhang Q, Huang S-Z, Jin J, Liu J, Li Y, Wang H-E, Chem L-H, Wang B-J, Su B-L (2016) Engineering 3D bicontinuous hierarchically macro-mesoporous $LiFePO_4$/C nanocomposite for lithium storage with high rate capability and long cycle stability. Sci Rep UK 6:1–12

[58] Guo H, Liu Y, Xi Y, Xu C, LQ, (2016) Investigation on high performance LiFePO4 nanoplates with the 010 face prominent for lithium battery cathode materials. Solid State Ion 298:44–50

[59] Zhao Y, Peng L, Liu B, Yu G (2014) Single-crystalline LiFePO$_4$ nanosheets for high-rate Li-ion batteries. Nano Lett 14:2849–2853

[60] Dokko K, Koizumi S, Nakano H, Kanamura K (2007) Particle morphology, crystal orientation, and electrochemical reactivity of LiFePO$_4$ synthesized by the hydrothermal method at 443 K. J Mater Chem 17:4803–4810

[61] Murugan AV, Muraliganth T, Manthiram A (2008) Comparison of microwave assisted solvothermal and hydrothermal syntheses of LiFePO$_4$/C nanocomposite cathodes for lithium ion batteries. J Phys Chem C 112:14665–14671

[62] Chen R, Wu Y, Kong XY (2014) Monodisperse porous LiFePO$_4$/C microspheres derived by microwave-assisted hydrothermal process combined with carbothermal reduction for high power lithium-ion batteries. J Power Sources 258:246–252

[63] Zhang L, Liang H (2013) Rapid synthesis of LiFePO$_4$ nanoparticles by microwave-assisted hydrothermal method. Russ J Electrochem 49:492–495